DOI: 10.1002/ ((please add manuscript number))
Article type: Full Paper

Title The Role of Metallic Dopants in Improving the Thermal Stability of the Electron Transport Layer in Organic Light-Emitting Diodes

*Chang-Min Keum, Nils M. Kronenberg, Caroline Murawski, Kou Yoshida, Yali Deng, Cordelia Berz, Wenbo Li, Mengjie Wei, Ifor D. W. Samuel, and Malte C. Gather**

Dr. C.-M. Keum, Dr. N. M. Kronenberg, Dr. C. Murawski, Dr. K. Yoshida, Y. Deng, C. Berz, W. Li, M. Wei, Prof. I. D. W. Samuel, Prof. M. C. Gather
Organic Semiconductor Centre, SUPA, School of Physics and Astronomy, University of St Andrews, St Andrews, KY16 9SS, United Kingdom
E-mail: mcg6@st-andrews.ac.uk

Keywords: organic light-emitting diodes, thermal stability, molecular doping, crystallization, atomic layer deposition

Abstract

4,7-Diphenyl-1,10-phenanthroline (BPhen) is widely used to create the electron transport layer (ETL) in organic light-emitting diodes (OLEDs) because of its high electron mobility and good compatibility with alkali metal n-dopants. However, the morphology of these ETLs is easily altered by heating due to the relatively low glass transition temperature of BPhen. Change in film morphology often reduces the electrical and optical performance of OLEDs and can lead to device failure. Here, we report on an enhancement in the thermal stability of OLEDs when doping their BPhen-based ETLs with cesium (Cs). To investigate the underlying mechanism and the role of the Cs dopant in the BPhen matrix, the crystallization features of Cs-doped BPhen films with different doping concentrations are characterized using optical microscopy and atomic force microscopy. In addition, the photophysical properties of the films, i.e., photoluminescence and absorbance, are examined. Next, the electrical and optical properties of blue fluorescent and red phosphorescent OLEDs containing BPhen layers with different Cs doping concentrations as ETL are characterized after annealing the OLEDs at temperatures ranging from 60 to 100 °C. Cs plays a critical role in inhibiting the undesired crystallization of BPhen thin films and therefore enhances the

thermal stability of OLEDs beyond the glass transition temperature of neat BPhen. Finally, highly stable BPhen-based OLEDs encapsulated by thin-film oxide layers grown via atomic layer deposition at 80 °C are demonstrated. This work may lead to a new strategy for enhancing the intrinsic thermal durability of organic devices and their compatibility with thermally demanding process conditions.

1. Introduction

Beyond the huge commercial success in the display market, e.g., for smartphones and televisions, organic light-emitting diode (OLED) technology is rapidly adapting to a multitude of promising new applications such as solid-state lighting,[1-3] flexible optoelectronics,[4] and more recently optogenetics[5] and medical therapies.[6] One of the main driving forces that has allowed OLEDs to enter commercial markets is the tremendous improvement in device lifetime and efficiency. However, ensuring robust stability in applications that require high luminance compared with typical displays (typical display luminance < 500 cd m^{-2}) remains challenging. Since the thermal conductivity of organic semiconductors is relatively low (typically, < 1 W m^{-1} K^{-1}),[7] and no efficient channel to dissipate heat is present in typical OLED stacks, resistive heating can be significant, particularly during high-brightness operation.[8] In addition to intrinsic resistive heating, heating can also occur due to environmental effects during OLED operation (e.g., when OLEDs are used in automotive applications) or due to the need for a certain process temperature during fabrication or encapsulation of devices. For instance, atomic layer deposition (ALD) is a promising technique to form thin, highly protective encapsulation layers that are intrinsically conformal and unlikely to be disrupted by local defects;[9] however, state-of-the-art ALD processes require a relatively high temperature during the deposition (typically, > 80 °C).[9-11] The influence of elevated temperature (due to either

resistive or external heating) on device performance has been extensively investigated and is seen as an important factor in OLED degradation.[12-14]

In general, an increase in temperature can induce morphological changes and may promote crystallization of one or several OLED layers, which in turn can reduce device performance and may lead to catastrophic failure via electric breakdown.[15] Because the thermal durability of organic materials is usually closely correlated to the glass transition temperature (T_g), a straightforward method to enhance device stability is to adapt existing materials for higher T_g or to develop new high-T_g materials.[16, 17] However, great care has to be taken to retain appropriate functionality of the material in the final OLED, e.g., in terms of charge transport or charge blocking performance. Another strategy is to blend an existing low-T_g material with a higher-T_g material. This can result in an intermediate T_g and thus in improved morphological stability of the film, even though this effect has been found to be relatively modest.[18] Given that state-of-the-art OLEDs generally comprise a multitude of layers, finding or synthesizing a set of suitable materials or material combinations that satisfy the specific requirements of each layer is challenging.

4,7-Diphenyl-1,10-phenanthroline (BPhen) has been widely used as an electron transport layer (ETL) in OLEDs because of its high electron mobility, deep lowest unoccupied molecular orbital level, and the possibility to further increase conductivity by n-doping e.g., with alkali metals[19-21] or alkali metal compounds.[22, 23] Naka et al. have reported that the electron mobility of BPhen is higher than for those of many other commonly used electron transport materials.[24] We found that BPhen-based OLEDs indeed show superior performance compared with those containing alternative ETL materials (e.g. NBPhen and TBPi, cf. **Figure S1**, Supporting Information). Thus, the use of BPhen is particularly desirable when OLEDs with high brightness and low power consumption are required.

However, due to the relatively low T_g of BPhen (62 °C),[25, 26] thin BPhen films tend to crystallize spontaneously,[26, 27] with thermal annealing further accelerating crystallization.[28]

Molecular doping is a key technique used to enhance the charge injection and electrical conductivity of charge transport layers in organic electronic devices.[29-31] Doping has been reported to inhibit molecular crystallization and thus to improve device lifetime;[28, 32] however, the effects of metallic dopants on thermal stability have not been studied. In addition, the mechanisms underlying the doping-induced resistance against crystallization have not been investigated in detail.

In this work, we report improved thermal stability of OLEDs with a BPhen ETL upon doping with cesium (Cs). The dependence of the crystallization features of thin films of BPhen on Cs doping concentration was investigated using optical microscopy and atomic force microscopy (AFM). We also examined the photophysical properties of the films, i.e., photoluminescence (PL) and absorbance. The PL spectra exhibited monotonic redshifts and broadening as the Cs doping concentration increased. Next, the electrical and optical properties of blue and red OLEDs containing BPhen ETLs with different Cs doping concentrations were characterized after annealing at temperatures between 60 and 100 °C. We find that aside from its conventional role of increasing the electrical conductivity of BPhen ETLs, Cs doping leads to marked increases in the thermal stability of the device. Finally, we show how this effect can be used to successfully encapsulate BPhen-based OLEDs with thin-film oxide layers using ALD.

2. Results and Discussion

2.1. Morphologies and Photophysical Properties of Cs-Doped BPhen Thin Films

To test the role of the Cs dopant in the BPhen matrix, we first investigated the crystallization features of 100 nm-thick Cs-doped BPhen films with different doping concentrations using

bright-field optical microscopy, epi-fluorescence microscopy, and AFM, as summarized in **Figure 1**.

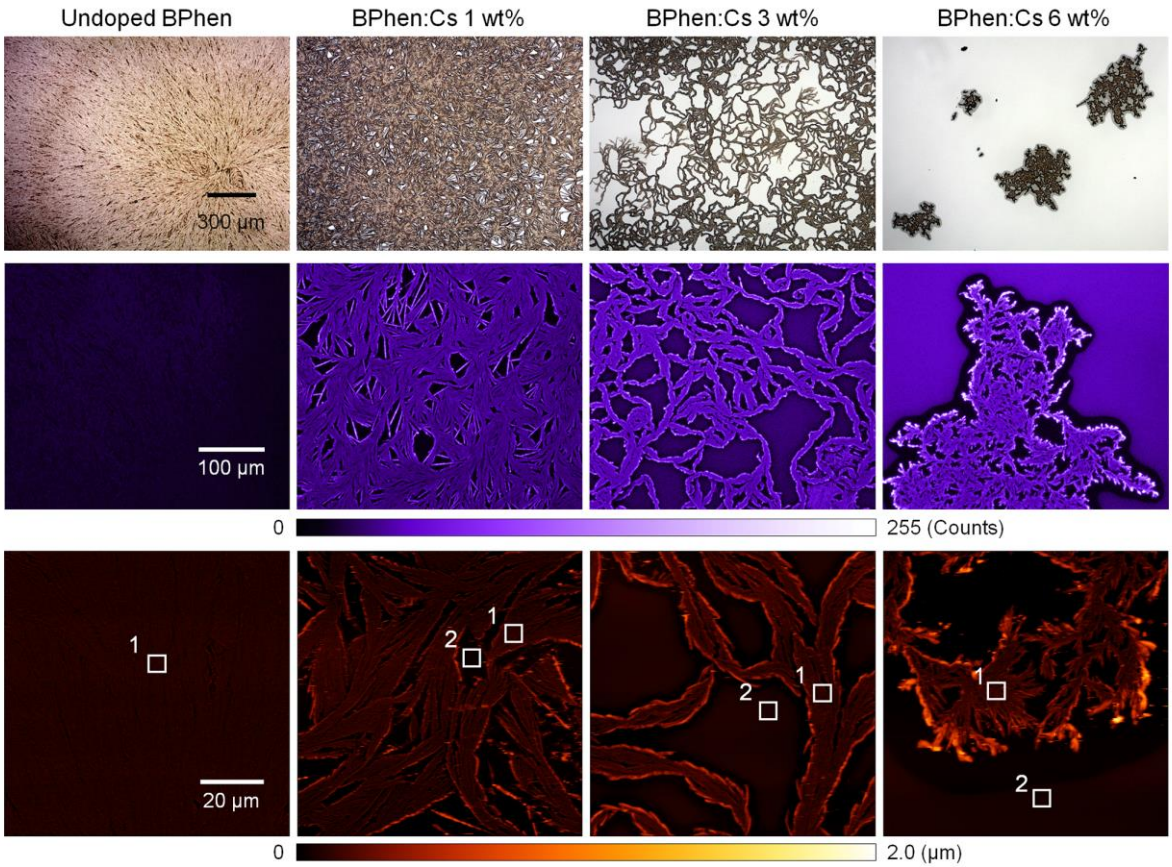

Figure 1. Bright-field optical microscopy (top row), epi-fluorescence (middle row) (excitation wavelength range, 310 nm < λ_{exc} < 390 nm with $\lambda_{exc\text{-}peak}$ = 360 nm; detection range, λ_{emi} > 420 nm), and AFM topography (bottom row) images of BPhen thin films, undoped and doped with three different Cs concentrations. In the AFM images, the white squares labelled 1 and 2 indicate crystallized and a non-crystallized areas, respectively (size, 5 × 5 µm²). All images were taken 4 weeks after the initial deposition of the films to allow sufficient time for crystallization (thickness, 100 nm).

Bright-field optical microscopy images (top row in Figure 1) clearly show that the entire undoped BPhen film has crystallized, and that the crystallized area decreases with increasing Cs doping concentration. The fraction of the crystallized area in each film was estimated by

image analysis (see Experimental), and the average fraction and standard deviation over five different fields of view are summarized in Table 1. The epi-fluorescence images (middle row in Figure 1) show an increase in detected fluorescence intensity with increased doping concentration. This increase is in part due to a redshift in emission as will be discussed in more detail in the next figure. The AFM measurements (bottom row in Figure 1) show that a higher Cs concentration results in a smoother surface within the amorphous regions of the film and a rougher surface where the film has crystallized. The surface roughness values of the crystallized and non-crystallized parts of the BPhen thin films highlighted with white squares in Figure 1 are summarized in Table 1. The material tends to agglomerate at the crystallite boundary, which leads to a reduction in the thickness of the surrounding areas (also see the dark areas in the epi-fluorescence images, especially for the BPhen:Cs 6 wt% sample). The thicknesses of the crystallized part of the film, of the edge of the crystallites, and of the area surrounding the crystallized regions were estimated to be approximately 200 nm, 600 nm, and 40 nm, respectively, in the BPhen:Cs 6 wt% film (**Figure S2**, Supporting Information).

Table 1. Fraction of the film that has crystallized (± standard deviation for five fields of view), and the surface roughness of the crystallized (1) and non-crystallized (2) regions highlighted in the AFM images in Figure 1 for BPhen films doped with different amounts of Cs.

	Fraction of crystallized area [%]	Roughness, root mean square [nm]	
		Crystallized (1)	Non-crystallized (2)
Undoped BPhen	100	14.85	-
BPhen:Cs 1 wt%	86.6 ± 2.4	25.89	3.71
BPhen:Cs 3 wt%	48.9 ± 11.3	35.19	2.42
BPhen:Cs 6 wt%	8.2 ± 1.9	44.66	1.99

We hypothesize that the Cs dopant acts as an impurity in the BPhen films that disturbs the molecular arrangement, and thus, prevents crystallization. This assumption is consistent with the observations described above. The patterns observed in the optical microscopy and AFM images suggest that Cs also interrupts uniform crystallite growth in the plane of the film, causing BPhen molecules to pile up at the edges of crystalline domains. For the undoped BPhen film, crystalline structures emerge from nuclei and then grow outwards radially, whereas more random structures are seen for the Cs-doped films (see bright-field optical microscopy images in Figure 1).

To further investigate the influence of Cs doping on BPhen thin films, we measured the absorption and PL spectra of undoped and Cs-doped BPhen thin films. (Note that the photophysical properties were measured immediately after the films were prepared, i.e., before substantial crystallization occurred.) With increasing concentration of Cs, the PL spectra of the BPhen films exhibit an increasing redshift and broadening, as shown in **Figure 2**. This redshift and broadening contributes to the apparent increase in brightness with Cs doping concentration in the epi-fluorescence images shown in Figure 1, i.e., the redshifted emission from the non-crystallized area of films with a higher Cs doping concentration is transmitted more efficiently by the filters used on the fluorescence microscope (transmission spectrum of the emission filter used; **Figure S3**, Supporting Information).

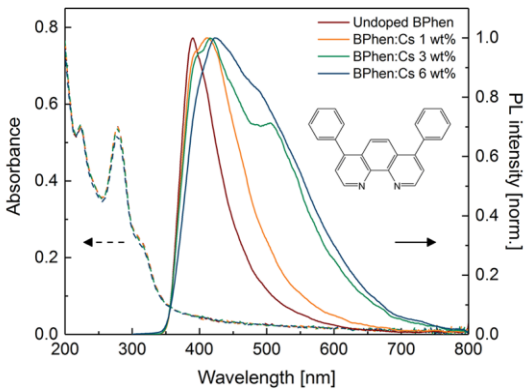

Figure 2. Absorption and normalized PL spectra (λ_{exc} = 278 nm) of BPhen thin films (thickness, 60 nm) with different Cs doping concentrations. The inset shows the molecular structure of BPhen.

Considering the molecular structure of BPhen (see the inset of Figure 2), when Cs is doped into the BPhen matrix, Cs ions will preferentially locate between the two nitrogen atoms of the BPhen molecule due to the strong metal ion coordinating property of 1,10-phenanthroline.[33-35] Previous studies on polymers containing phenanthrolines or structurally related units have found changes in the emission spectra for polymer-metal mixtures and have attributed this effect to metal ion chelation.[36, 37] Thus, the spectral redshifts observed with increasing Cs-doping of BPhen thin films seen here might also be due to the formation of metal coordination complexes, during which Cs atoms oxidize and donate electrons to BPhen molecules. This complex formation may effectively prevent further crystallization between neighboring BPhen molecules as the film now contains a mixture of two different molecular species, in which the formation of BPhen crystallites may be kinetically hindered by the need for metal coordination complexes to diffuse out before crystallization can occur.

In contrast to the PL spectra, the absorbance spectra do not change with Cs doping concentration. This indicates that the emission originates from a relatively small number of trap sites, i.e., excitons formed by absorption on non-metal coordinating, pristine BPhen molecules may diffuse to traps before decaying. As the trap density is low, presumably due to limited efficiency of Cs doping in BPhen (analogous to other n-doping systems[38, 39]) the number of traps in the film is too small to influence the absorption spectrum by a notable amount.

2.2. Thermal Stability of OLEDs

Next, we examined the use of Cs-doped BPhen as ETL in blue and red OLED p-i-n stacks, i.e., OLEDs consisting of a p-doped layer, intrinsic layers, and an n-doped layer. The Cs doping concentration was varied in the same manner as for the thin-film studies above. Both types of OLEDs use the same materials for each functional layer – except for the emissive layer (EML), which was MADN doped with TBPe (fluorescent emitter) for the blue OLEDs (**Figure 3**a) and NPB doped with $Ir(MDQ)_2(acac)$ (phosphorescent emitter) for the red OLEDs (Figure 3d) (see experimental section for details). The current density-luminance vs. voltage characteristics for un-treated and annealed blue and red OLEDs are also shown in Figure 3. For the un-treated OLEDs even 1 wt% Cs doping dramatically increases current density and luminance (Figure 3b and e). However, current density and luminance do not show a significant further increase for higher doping concentrations, indicating that a small amount of doping is sufficient to improve the electrical conductivity of the BPhen layer and the charge injection at the cathode contact to a point where they are no longer the limiting factor for the overall current passing through the OLED. Diffusion of Cs into the EML would likely lead to exciton quenching. The fact that no reduction in device performance is observed with increasing Cs doping indicates that the undoped BAlq layer between the EML and the doped ETL provides an efficient buffer, supressing exciton quenching by Cs in our OLEDs. This observation is consistent with a previous report.[19]

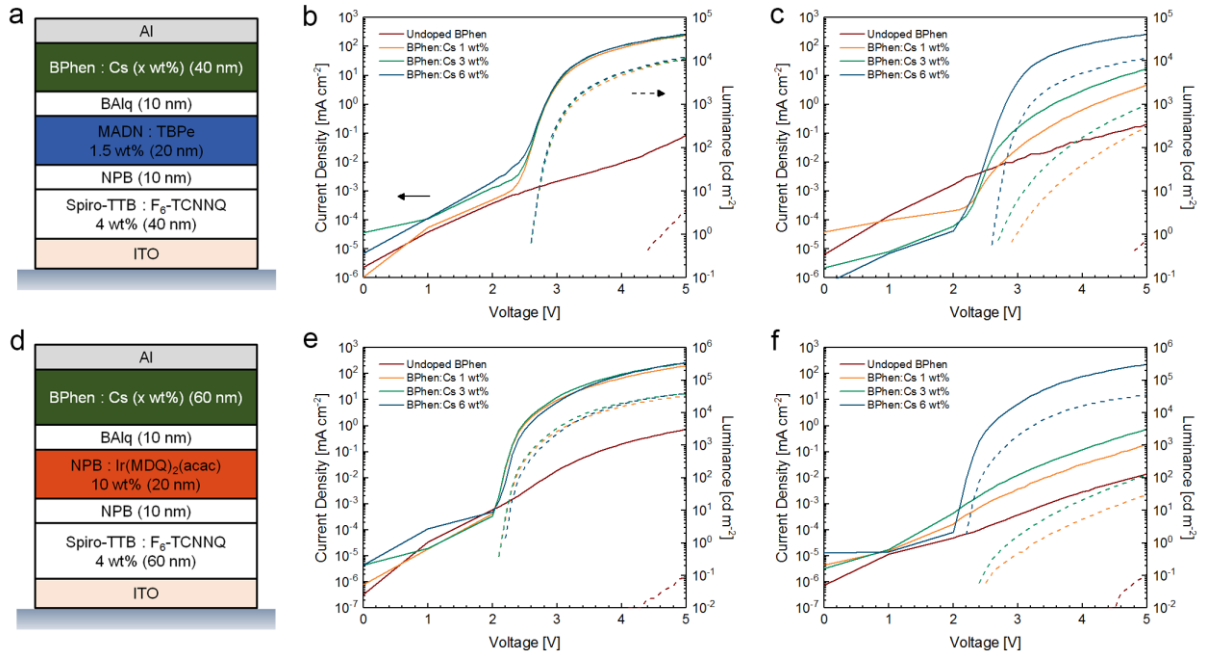

Figure 3. Layer structures of the p-i-n type (a) blue and (d) red OLED stacks used here. Current density (solid lines) and luminance (dashed lines) vs. voltage characteristics for blue OLEDs with different Cs doping concentrations in the BPhen ETL that are (b) un-treated and (c) annealed at 80 °C; same for red OLEDs, (e) un-treated and (f) annealed at 80 °C.

After annealing the OLEDs at 80 °C for 60 min, the current density-luminance vs. voltage characteristics of the OLEDs with an undoped or weakly doped BPhen layer changed dramatically, with substantially reduced current and brightness compared with those obtained before annealing (Figure 3c and f). However, for the OLED with a 6 wt% Cs-doped BPhen layer, no significant reduction in current and brightness is observed. Given that thermal annealing is known to induce a reorganization of organic molecules and to promote crystallization[28] and considering our observations above, we propose that the improved thermal stability is closely related to the reduction in crystallization when Cs is present in the BPhen layer. To rationalize these results more quantitatively, it is worth to consider the molar ratio, i.e., the ratio of the number of dopant molecules to the number of matrix molecules. The used doping concentrations of 1, 3, and 6 wt% correspond to molar ratios of 0.025, 0.077,

and 0.16, respectively, i.e., there is one Cs atom for every 40 BPhen molecules in 1 wt% doped films, and one per every 6 to 7 BPhen molecules in the 6 wt% case.

Figure 4 summarizes the current density and luminance results of the blue and red OLEDs prior to and after annealing at temperatures between 60 and 100 °C. Both the blue and red OLEDs show a similar systematic trend: the annealing temperature above which the current density and luminance begin to drop is higher for OLEDs with higher Cs doping concentration in the BPhen ETL. This effect is very strong; while devices with 1 wt% doping show a 10- to 100-fold loss in current density and luminance, there is virtually no reduction in performance for OLEDs with a BPhen ETL with 6 wt% Cs doping after annealing at 80 °C, i.e., at a temperature higher than the T_g of BPhen (62 °C). OLEDs with an undoped BPhen ETL show a poor current and luminance performance even prior to annealing; their current but not their luminance increases upon annealing at ≥ 80 °C. This increase is ascribed to a drastically increased leakage current due to the deformation of the BPhen layer. After annealing at 100 °C, none of the OLEDs, except for those with 6 wt% Cs doping, show measurable emission anymore (Figure 4b and d).

The results shown in Figure 3 and 4 are in good agreement with the doping concentration dependence of crystallization features discussed in Section 2.1. Thus, Cs doping plays a critical role, not only in preventing the undesired crystallization of BPhen molecules in a thin film, but also in improving the thermal stability of OLEDs containing a BPhen layer.

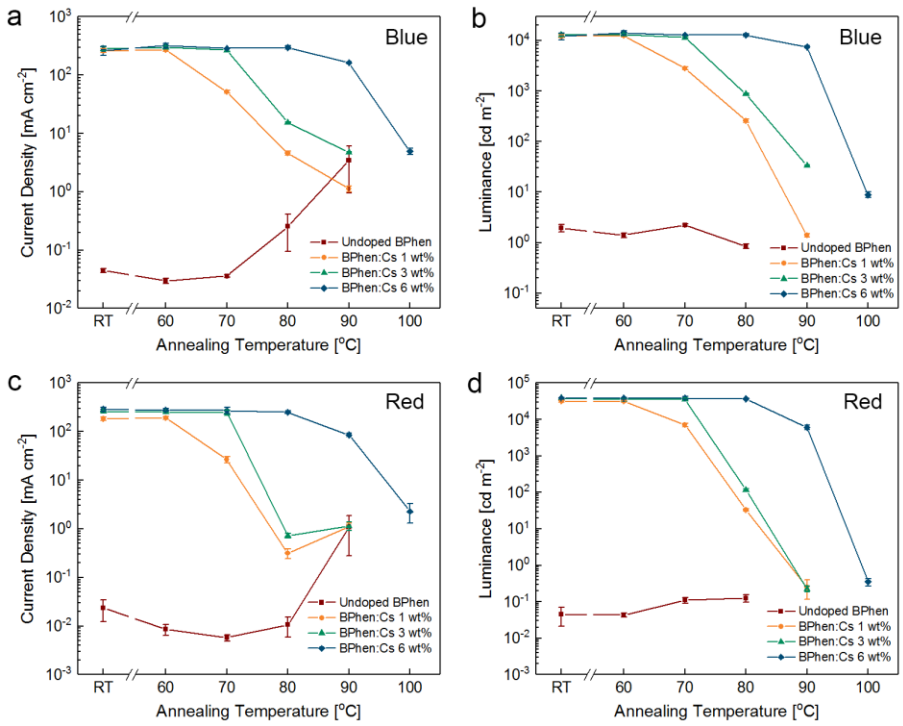

Figure 4. Variation in (a), (c) current density and (b), (d) luminance at a 5 V bias voltage vs. annealing temperature applied to (a), (b) blue and (c), (d) red OLEDs. Data points and error bars represent the average and standard deviation of 5 OLED pixels.

Figure 5a and b show a comparison of the EQE and normalized EL spectra of the blue and red OLEDs with BPhen:Cs 6 wt% after annealing at different temperatures, respectively (see **Figure S4**, Supporting Information for the corresponding current density-luminance vs. voltage characteristics). The EQE of both the blue and red OLEDs do not substantially decrease for annealing temperatures up to 80 °C. After annealing at 90 °C, the EQEs of the red OLEDs decrease dramatically, in particular in the high current density regime. In contrast, the EQE values of the blue OLEDs are only weakly affected by annealing at 90 °C. This difference is attributed to the relatively low T_g of the host material used in the EML of the red OLEDs (NPB, T_g = 95 °C[40]) compared with the EML host material in the blue OLEDs (MADN, T_g = 120 °C[41]). Annealing at temperatures close to the host T_g will likely result in molecular segregation of the Ir(MDQ)$_2$(acac) emitter molecules, which then

leads to inefficient host-guest energy transfer as well as to significant triplet-triplet annihilation. The shapes of the EL spectra are not affected by the annealing at any of the investigated temperatures (up to 90 °C), as shown in Figure 5b. This confirms that the energy levels of the organic materials involved in radiative recombination are not altered and that the optical cavity structure of the OLED is not substantially deformed by the thermal annealing, even though ETL and EML morphology begin to change for the highest of the tested annealing temperatures.

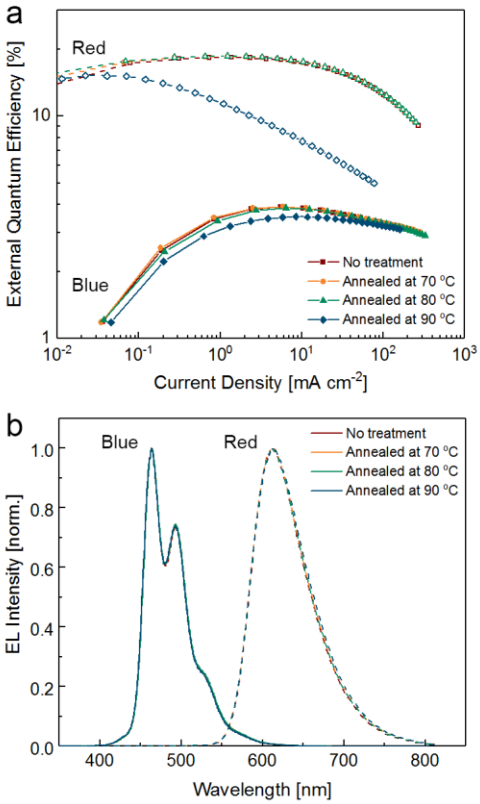

Figure 5. (a) EQE and (b) normalized EL spectra of blue (closed symbols, solid lines) and red (open symbols, dashed lines) OLEDs with an ETL of BPhen:Cs (6 wt%) after annealing the devices at different temperatures.

A further increase in doping concentration to 9 wt% improves the thermal stability further, but at the cost of substantially decreased electrical and optical performance (**Figure**

S5, Supporting Information). For example, the relative reduction in luminance at 5 V after annealing at 90 °C ((L_0 - $L_{90°C}$)/L_0) are only 15% and 22% for blue and red OLEDs with 9 wt% doping, respectively; compared with 39% and 84% for 6 wt% doping. This also indicates that the BAlq layer is not altered and that it continues to efficiently block diffusion of Cs atoms and excitons even after annealing at a temperature close to the T_g of BAlq (92 °C[18]). However, the absolute device performance for OLEDs with 9 wt% Cs doping is significantly lower than for the OLEDs with lower doping concentrations discussed in Figure 3-5 (e.g., 1.3-2.0 fold for current and 2.4-4.0 fold for luminance at 5 V). Hence, the doping concentration must be carefully optimized and controlled to achieve high thermal stability without compromising device performance.

Finally, we demonstrate the encapsulation of blue and red OLEDs with thin-film oxide layers that were grown at 80 °C using ALD. Both the blue and red OLEDs utilized BPhen layers doped with 6 wt% Cs. Alternating layers of Al_2O_3 and ZrO_2 were deposited directly onto the fabricated OLED stacks, following the protocol described in the experimental section. Compared with Al_2O_3 alone, Al_2O_3/ZrO_2 hybrid layers have been reported to show superior device protection in terms of the water-vapor and oxygen transmission rates.[9]

As expected, the current density-luminance vs. voltage characteristics and EQE are not significantly affected by ALD encapsulation (**Figure S6**, Supporting Information). The operational lifetime of the ALD-encapsulated OLEDs is compared with otherwise identical OLEDs that were encapsulated with conventional getter-embedded glass lids. **Figure 6** shows the decrease in relative luminance for the blue and red OLEDs when under a constant current stress of J = 20 mA cm^{-2} and 5 mA cm^{-2}, respectively. The initial luminance values at these current densities are ~1200 cd m^{-2} for the blue OLEDs and ~1300 cd m^{-2} for the red OLEDs. No substantial difference in device degradation is observed between ALD-encapsulated

OLEDs and OLEDs encapsulated with glass lids, although the luminance of the ALD-encapsulated red OLEDs decay slightly faster after 100 h of continuous operation.

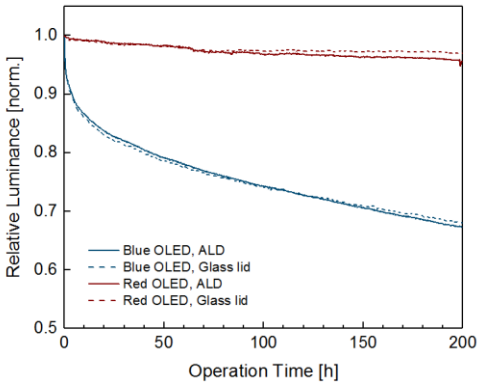

Figure 6. Lifetimes of the blue and red OLEDs (BPhen:Cs 6 wt%) encapsulated with thin-film oxide layers using ALD (straight lines) or with getter-embedded cavity glass lids (dashed lines). The relative luminance over the operation time was measured under a constant bias stress of J = 20 mA cm^{-2} for the blue OLEDs and 5 mA cm^{-2} for the red OLEDs.

3. Conclusion

In conclusion, Cs plays a critical role in inhibiting the undesired crystallization of thin films of BPhen film and in enhancing the thermal stability of BPhen-based ETLs beyond the T_g of neat BPhen. The role of the Cs dopant in the BPhen matrix and the underlying mechanism were elucidated by investigating the crystallization features of Cs-doped BPhen films with different doping concentrations using optical microscopy and AFM, as well as by examining the photophysical properties of the films, including photoluminescence and absorption. We found that the thermal stability of OLEDs with BPhen ETLs can be markedly improved by Cs doping, but the doping concentration must be carefully optimized to simultaneously obtain optimum thermal stability and device performance; for the devices studied here, the optimum Cs doping concentration is 6 wt%. Based on these findings, we successfully demonstrated stable BPhen-based OLEDs that were encapsulated with thin-film oxide layers deposited by

ALD. To further improve the understanding of the behaviour of metallic dopants in organic host materials, particularly those with metal-coordinating groups, investigations on different organic-metal doping systems are needed. In addition, it will be interesting to see if our results for Cs doping can be transferred to Cs compounds like Cs_2CO_3.[22, 23] However, the present results may be transferable to other material systems, and thus, may pave the way for enhancing the intrinsic thermal durability of organic devices and their compatibility with processes involving thermal treatments.

4. Experimental Section

Thin-Film Characterization: 100 nm-thick films of BPhen, doped with Cs at nominal concentrations of 0, 1, 3, and 6 wt% were prepared by thermal co-evaporation onto cleaned glass substrates in a vacuum chamber (EvoVac, Angstrom Engineering Inc.) at a base pressure of 2×10^{-7} mbar. The Cs doping concentration was estimated from the evaporation rates of BPhen and Cs, which were individually monitored by two quartz crystal microbalances. The prepared thin films were observed with a bright-field optical microscope (Axio Lab.A1, Zeiss) and an inverted epi-fluorescence microscope (Ti Eclipse, Nikon) with a Hg light source and a DAPI filter cube (see Figure S3, Supporting Information for transmission spectra). The background emission from a blank glass substrate was subtracted from the recorded images. To quantify the fraction of the crystallized area, the microscopy images were converted to binary images and analyzed using the image processing software ImageJ. AFM topography maps of the BPhen thin films were acquired under ambient conditions using contact mode AFM (FlexAFM system, Nanosurf) with tipped cantilevers (ContAl-G) and a force set point of 10 nN.

Photophysical properties were measured on 60 nm-thick undoped and Cs-doped films. Absorption spectra were measured using a UV−vis spectrophotometer (Cary 300, Varian),

and PL spectra in the wavelength region between 300 and 800 nm were recorded using a spectrometer with the excitation wavelength set to 278 nm (FLS980, Edinburgh Instruments).

OLED Fabrication and Characterization: The acronyms of the materials used in the OLED stacks are as follows. Spiro-TTB: 2,2',7,7'-tetrakis-(*N*,*N*-di-methylphenylamino)-9,9'-spiro-bifluorene, F_6-TCNNQ: 2,2'-(perfluoronaphthalene-2,6-diylidene)dimalononitrile, NPB: *N*,*N*'-bis(naphthalen-1-yl)-*N*,*N*'-bis(phenyl)-benzidine, MADN: 2-methyl-9,10-bis(naphthalen-2-yl)anthracene, TBPe: 2,5,8,11-tetra-tert-butylperylene, $Ir(MDQ)_2(acac)$: (2-methyldibenzo[*f*,*h*]quinoxaline)(acetylacetonate)iridium(III), BAlq: bis(2-methyl-8-quinolinolate)-4-(phenylphenolato)aluminum, BPhen: 4,7-diphenyl-1,10-phenanthroline, NBPhen: 2,9-dinaphthalen-2-yl-4,7-diphenyl-1,10-phenanthroline, TPBi: 2,2',2''-(1,3,5-benzinetriyl)-tris(1-phenyl-1-*H*-benzimidazole).

To fabricate blue and red p-i-n OLEDs, the following layers were deposited on indium-tin-oxide (ITO)-structured glass substrates from bottom to top: Spiro-TTB doped with F_6-TCNNQ at 4 wt% (40 nm for blue OLEDs and 60 nm for red OLEDs) as hole transport layer (HTL) / NPB (10 nm) as electron blocking layer (EBL) / MADN doped with TBPe at 1.5 wt% as EML (20 nm) for the blue OLEDs and NBP doped with $Ir(MDQ)_2(acac)$ at 10 wt% as EML for the red OLEDs / BAlq (10 nm) as hole blocking layer (HBL) / BPhen doped with 0, 1, 3, 6, or 9 wt% of Cs (40 nm for the blue OLEDs and 60 nm for the red OLEDs) as ETL / Al (100 nm) as cathode. The thicknesses of the HTL and ETL in the blue and red OLEDs were selected to provide optimal light extraction. NBPhen and TPBi were also used as alternative ETL materials instead of BPhen for a comparison of device performances (see Figure S1, Supporting Information). The effective pixel area of all devices was 4 mm × 4 mm. After deposition of the OLED stack, devices were directly transferred into a nitrogen glovebox without intermittent exposure to air and then encapsulated with either getter-embedded cavity glass lids attached by a UV-curable epoxy glue or thin-film oxide layers

using an ALD reactor (Savannah S200, Ultratech). The oxide encapsulation barriers (total thickness, 150 nm) were prepared by alternating depositions of Al_2O_3 and ZrO_2 sublayers (3 nm each). To grow the Al_2O_3 sublayers, trimethylaluminum (TMA) and H_2O precursors were repeatedly pulsed for 15 ms each with 10 s N_2 purging intervals in between (20 sccm) (20 cycles). A pulse recipe of tetrakis(dimethylamino)zirconium (TDMAZr) for 0.3 s and H_2O for 30 ms with 7 s N_2 purging intervals (28 cycles) was used for the ZrO_2 sublayers. The TDMAZr cylinder was heated to 75 °C, while the TMA and H_2O precursors were maintained at room temperature. The temperature and base pressure of the ALD reactor were 80 °C and 0.1 torr, respectively. To investigate the thermal stability of OLEDs, they were annealed at temperatures between 60 and 100 °C in the ALD reactor for 60 min at the base pressure of 0.1 torr.

The electrical and optical characteristics of our OLEDs were measured using a source-measurement unit (Keithley 2400, Keithley) and a calibrated silicon photodiode. Electroluminescence (EL) spectra of the OLED emission were obtained using a spectrograph (MS125^{TM}, Oriel) coupled to a CCD camera (DV420-BU, Andor). Efficiencies were calculated assuming a Lambertian emission profile. The lifetime of the OLEDs was measured by monitoring the relative luminance over time at a constant current using a silicon photodiode (PDA100A-EC, Thorlabs).

Supporting Information
Supporting Information is available from the Wiley Online Library or from the author.

Acknowledgements
This research was financially supported by the EPSRC NSF-CBET lead agency agreement (EP/R010595/1, 1706207), the DARPA-NESD program (N66001-17-C-4012) and by the EPSRC CDT Capital Equipment funding stream (EP/L017008/1). C.-M.K. acknowledges support from Basic Science Research Program through the National Research Foundation of Korea (NRF) funded by the Ministry of Education (2017R1A6A3A03012331). C.M. acknowledges funding by the European Commission through a Marie Skłodowska Curie Individual Fellowship (703387). Y.D., W.L., and M.W. acknowledge stipends from the

Chinese Scholarship Council (CSC). I.D.W.S. acknowledges support from a Royal Society Wolfson research merit award.

Received: ((will be filled in by the editorial staff))
Revised: ((will be filled in by the editorial staff))
Published online: ((will be filled in by the editorial staff))

References

[1] B. W. D'Andrade, S. R. Forrest, *Adv. Mater.* **2004**, *16*, 1585.

[2] K. T. Kamtekar, A. P. Monkman, M. R. Bryce, *Adv. Mater.* **2010**, *22*, 572.

[3] M. C. Gather, S. Reineke, *J. Photon. Energy* **2015**, *5*, 057607.

[4] T.-H. Han, Y. Lee, M.-R. Choi, S.-H. Woo, S.-H. Bae, B. H. Hong, J.-H. Ahn, T.-W. Lee, *Nat. Photonics* **2012**, *6*, 105.

[5] A. Morton, C. Murawski, S. R. Pulver, M. C. Gather, *Sci. Rep.* **2016**, *6*, 31117.

[6] A. K. Bansal, S. Hou, O. Kulyk, E. M. Bowman, I. D. Samuel, *Adv. Mater.* **2015**, *27*, 7638.

[7] X. Y. Wang, K. D. Parrish, J. A. Malen, P. K. L. Chan, *Sci. Rep.* **2015**, *5*, 16095.

[8] A. Fischer, T. Koprucki, K. Gärtner, M. L. Tietze, J. Brückner, B. Lüssem, K. Leo, A. Glitzky, R. Scholz, *Adv. Funct. Mater.* **2014**, *24*, 3367.

[9] J. Meyer, P. Görrn, F. Bertram, S. Hamwi, T. Winkler, H.-H. Johannes, T. Weimann, P. Hinze, T. Riedl, W. Kowalsky, *Adv. Mater.* **2009**, *21*, 1845.

[10] S. M. George, *Chem. Rev.* **2010**, *110*, 111.

[11] V. Vandalon, W. M. M. Kessels, *Appl. Phys. Lett.* **2016**, *108*, 011607.

[12] M. Ishii, Y. Taga, *Appl. Phys. Lett.* **2002**, *80*, 3430.

[13] X. Zhou, J. He, L. S. Liao, M. Lu, X. M. Ding, X. Y. Hou, X. M. Zhang, X. Q. He, S. T. Lee, *Adv. Mater.* **2000**, *12*, 265.

[14] K. Yoshida, H. Nakanotani, C. Adachi, *Org. Electron.* **2016**, *31*, 287.

[15] S. Scholz, D. Kondakov, B. Lüssem, K. Leo, *Chem. Rev.* **2015**, *115*, 8449.

[16] F. Steuber, J. Staudigel, M. Stossel, J. Simmerer, A. Winnacker, H. Spreitzer, F. Weissortel, J. Salbeck, *Adv. Mater.* **2000**, *12*, 130.

[17] S. Tokito, H. Tanaka, K. Noda, A. Okada, Y. Taga, *Appl. Phys. Lett.* **1997**, *70*, 1929.

[18] B. W. D'Andrade, S. R. Forrest, A. B. Chwang, *Appl. Phys. Lett.* **2003**, *83*, 3858.

[19] G. F. He, O. Schneider, D. S. Qin, X. Zhou, M. Pfeiffer, K. Leo, *J. Appl. Phys.* **2004**, *95*, 5773.

[20] R. Meerheim, K. Walzer, M. Pfeiffer, K. Leo, *Appl. Phys. Lett.* **2006**, *89*, 061111.

[21] S. Reineke, F. Lindner, G. Schwartz, N. Seidler, K. Walzer, B. Lüssem, K. Leo, *Nature* **2009**, *459*, 234.

[22] J. Zhao, Y. Cai, J. P. Yang, H. X. Wei, Y. H. Deng, Y. Q. Li, S. T. Lee, J. X. Tang, *Appl. Phys. Lett.* **2012**, *101*, 193303.

[23] K. P. Guo, C. F. Si, C. Han, S. H. Pan, G. Chen, Y. Q. Zheng, W. Q. Zhu, J. H. Zhang, C. Sun, B. Wei, *Nanoscale* **2017**, *9*, 14602.

[24] S. Naka, H. Okada, H. Onnagawa, T. Tsutsui, *Appl. Phys. Lett.* **2000**, *76*, 197.

[25] J.-H. Lee, M.-H. Wu, C.-C. Chao, H.-L. Chen, M.-K. Leung, *Chem. Phys. Lett.* **2005**, *416*, 234.

[26] Y. H. Choi, Y. P. Jeon, D. C. Choo, T. W. Kim, *Org. Electron.* **2015**, *22*, 197.

[27] T. Maindron, J.-Y. Simon, E. Viasnoff, D. Lafond, *Thin Solid Films* **2012**, *520*, 6876.

[28] S.-Y. Chen, T.-Y. Chu, J.-F. Chen, C.-Y. Su, C. H. Chen, *Appl. Phys. Lett.* **2006**, *89*, 053518.

[29] K. Walzer, B. Maennig, M. Pfeiffer, K. Leo, *Chem. Rev.* **2007**, *107*, 1233.

[30] B. Lüssem, C. M. Keum, D. Kasemann, B. Naab, Z. N. Bao, K. Leo, *Chem. Rev.* **2016**, *116*, 13714.

[31] C. Gaul, S. Hutsch, M. Schwarze, K. S. Schellhammer, F. Bussolotti, S. Kera, G. Cuniberti, K. Leo, F. Ortmann, *Nat. Mater.* **2018**, *17*, 439.

[32] L. S. Liao, K. P. Klubek, *US 7211948 B2*, **2007**.

[33] J. Kido, H. Hayase, K. Hongawa, K. Nagai, K. Okuyama, *Appl. Phys. Lett.* **1994**, *65*, 2124.

[34] J. Kido, T. Matsumoto, *Appl. Phys. Lett.* **1998**, *73*, 2866.

[35] T. Yamamoto, Y. Saitoh, K. Anzai, H. Fukumoto, T. Yasuda, Y. Fujiwara, B. K. Choi, K. Kubota, T. Miyamae, *Macromolecules* **2003**, *36*, 6722.

[36] T. Yasuda, T. Yamamoto, *Macromolecules* **2003**, *36*, 7513.

[37] T. Yasuda, I. Yamaguchi, T. Yamamoto, *Adv. Mater.* **2003**, *15*, 293.

[38] C. K. Chan, E. G. Kim, J. L. Bredas, A. Kahn, *Adv. Funct. Mater.* **2006**, *16*, 831.

[39] M. L. Tietze, P. Pahner, K. Schmidt, K. Leo, B. Lüssem, *Adv. Funct. Mater.* **2015**, *25*, 2701.

[40] D. F. O'Brien, P. E. Burrows, S. R. Forrest, B. E. Koene, D. E. Loy, M. E. Thompson, *Adv. Mater.* **1998**, *10*, 1108.

[41] Z. Y. Yang, Z. G. Chi, T. Yu, X. Q. Zhang, M. N. Chen, B. J. Xu, S. W. Liu, Y. Zhang, J. R. Xu, *J. Mater. Chem.* **2009**, *19*, 5541.

Table of contents text:

Controlling the cesium doping concentration in electron transport layers is found to improve the thermal stability of organic light-emitting diodes (OLEDs) by preventing crystallization. Using the electron transport material BPhen as an example, crystallization is investigated by morphological and photophysical characterization of thin films annealed at different temperatures. The improved thermal stability of OLEDs allows the use of high-temperature processes, such as thin-film encapsulation by atomic layer deposition.

Keyword organic light-emitting diodes, thermal stability, molecular doping, crystallization, atomic layer deposition

C.-M. Keum, N. M. Kronenberg, C. Murawski, K. Yoshida, Y. Deng, C. Berz, W. Li, M. Wei, I. D. W. Samuel, M. C. Gather*

Title The Role of Metallic Dopants in Improving the Thermal Stability of the Electron Transport Layer in Organic Light-Emitting Diodes

ToC figure